Statistical mechanical simulations on properties of liquid pyridine

Kritsana Sagarik [a,*], Eckhard Spohr [b]

[a] *School of Chemistry, Institute of Science, Suranaree University of Technology, Nakhon Ratchasima 30000, Thailand*
[b] *Abteilung für Theoretische Chemie, Universität Ulm, D-7900 Ulm, Germany*

Abstract

An intermolecular potential describing the interaction between pyridine molecules was constructed using the test-particle model (T-model). The computed T-model potential was used in the investigation of the equilibrium structures and binding energies of pyridine dimers. It was found that a herringbone structure is the most stable dimer in the gas phase. The results of the statistical mechanical simulations revealed that this dimer structure may not be present in an appreciable amount in the liquid phase. The molecular dynamics (MD) simulations confirmed that the molecular motions of pyridine in the liquid phase are rather anisotropic, as can be seen from the computed rotational diffusion constants. This finding is in good agreement with the experimental investigation on reorientational motions of pyridine reported by Kintzinger and Lehn.

1. Introduction

Intermolecular potentials are required as the primary input for many kinds of statistical mechanical simulations. The advancement of computer technology nowadays allows computational chemists to compute intermolecular potentials for larger molecules with more acceptable accuracies. However, the computational models employed for such molecules are still limited to ab initio calculations at the Hartree–Fock level of theory, at which the effects of electron correlation are neglected. The applications of ab initio calculations that include the effects of electron correlation, in a supermolecular fashion, are still restricted to small molecules due to the limit of computer resources. For molecules with

electronic resonance forms, such as aromatic and heterocyclic compounds, the effects of electron correlation cannot be neglected. Therefore, ab initio calculations at the Hartree–Fock level of theory are inadequate.

In the previous publications [1–4], an attempt has been made to derive intermolecular potentials using first-order perturbation theories. It was named test-particle model (T-model) [1] since the major energy contributions to the intermolecular potential are deduced separately by probing molecules of interest with suitable test particles. This reduces the degrees of freedom used to describe the relative positions and orientations of each pair of molecules from six, as in the case of supermolecular approach, to only three. The potential parameters derived in this way are considered to be site parameters and, therefore, transferable. The major advantage of the T-model over the Hartree–Fock SCF calculations is that the

---

* Corresponding author.

T-model includes the effects of electron correlation in an approximate way. This makes the T-model appropriate for molecules, in which the effects of electron correlations cannot be neglected. The T-model has been tested in various chemical systems, ranging from diatomic molecules to the base pairs of DNA [2–5]. The computed T-model potentials have been applied successfully in molecular dynamics (MD) simulations of liquid properties [2,3,5].

Pyridine has been used as a solvent and starting material in chemical synthesis [6]. Being a nitrogen heterocyclic compound with the dipole moment of about 2.2 D makes physical and chemical properties of pyridine different from those of benzene, for which a number of theoretical and experimental results have been well documented [7,8]. Molecular motions in liquid pyridine have been studied mainly using NMR techniques [9–15]. Kintzinger and Lehn [9] investigated molecular dynamics of liquid pyridine using deuterium and ^{14}N nuclear quadrupolar relaxation methods. They concluded that the molecular motions of pyridine are anisotropic and the anisotropy changes from solid-like to gas-like as the temperature increases. They also suggested that at low temperature the molecular reorientations may be described as a rotational diffusion process. O'Reilly, Peterson and Yasaitis [15] measured the self-diffusion coefficients of pyridine at various temperatures, ranging from the freezing point to the normal boiling point. From the values of τ_2, the authors believed that the anisotropy of liquid pyridine reported by Kintzinger and Lehn is unreasonable. A MD study of liquid pyridine has been reported by Gamba and Klein [16]. The MD results revealed a strong coupling between translational and rotational motion in the liquid phase. However, after making comparison with available experimental data, the authors concluded that the intermolecular potential employed in MD might be inadequate.

In the present report, a T-model potential was constructed for pyridine. The potential was employed to determine the equilibrium structures of pyridine dimer in the gas phase. Liquid pyridine was studied at various temperatures by means of Monte Carlo (MC) and MD simulations. The structural and dynamic properties were discussed in comparison with the aforementioned theoretical and experimental results.

2. Methods

In this section all theoretical methods employed in the present study are briefly summarized.

2.1. Test-particle model (T-model)

As mentioned earlier, supermolecule ab initio calculations are suitable only for small molecules with high symmetry. Previous experience [17] has shown that thousands of dimer configurations must be computed when the intermolecular potentials to describe DNA bases/H_2O interaction were constructed using supermolecular approach, and each dimer configuration needed about two CPU hours in IBM 3090 supercomputers. Ahlrichs and his coworkers [1] put forward a theoretical method for intermolecular potential calculations. The method has been regarded as 'the test-particle model' or T-model. Since the T-model is based on first-order perturbation theories, it demands less computing power, in comparison with ab initio calculations in supermolecular approach. Within the framework of the T-model, each energy contribution to the intermolecular interaction energy is computed separately by probing the molecule of interest with suitable test particles. The T-model had been used to study structural and dynamic properties of halogenated methanes [5], and has been applied successfully in the study of weak and moderately strong hydrogen-bonded systems, such as liquid ammonia [2] and liquid formamide [3], as well as aqueous solutions of formamide [18].

The intermolecular interaction energy in the T-model is written as

$$\Delta E = \Delta E_{scf}^1 + \Delta E^r. \tag{1}$$

ΔE_{scf}^1 is the first-order interaction which represents the exchange and Coulombic energies. ΔE_{scf}^1 is approximated by the following site–site expression:

$$\Delta E_{scf}^1 = \sum_{i \in A} \sum_{j \in B} \exp\left(\frac{-R_{ij} + \sigma_i + \sigma_j}{\rho_i + \rho_j}\right) + \frac{q_i q_j}{R_{ij}}, \tag{2}$$

where i and j label the sites of molecules and σ_i, ρ_i and q_i are site parameters. The exponential term in Eq. (2) is the repulsion part of the potential. The exponential parameters in Eq. (2) are determined by

probing the molecules of interest (for example molecules A and B) in various directions with an uncharged spherical test particle. A nitrogen in its average of terms state has been proved to be the most suitable [1]. In practice, ab initio wavefunctions at the Hartree–Fock level of theory of monomers A and B have to be computed first. Then the repulsive energies between A, as well as B, and the test particle are computed from the wavefunctions by means of first-order perturbation theories. These repulsive energies are used to determine the exponential parameters σ_i and ρ_i, by means of least square fits and combination rules. The point charges q_i and q_j are determined in the same way namely, by probing molecule A, as well as B, with a point charge q. The results are electrostatic potential energies (V_A and V_B) in the vicinities of A and B, respectively. q_i and q_j are determined to reproduce V_A and V_B by least square fits. The point charges computed in this manner are similar to the ones obtained from the potential derived method (PD method) [19].

Williams and Weller [20] reported the PD charges for various azabenzene molecules. The PD charges were deduced from SCF-MO calculations with 6-31G basis set. Orozco and Luque [21] reported electrostatic charges for pyridine. The charges were deduced from a slightly larger basis set, 6-31G *. Both sets of electrostatic charges were tested in Eq. (2). It was found that they gave nearly the same results. Only the results obtained with the charges given by Orozco and Luque are reported in the present study.

ΔE^r in Eq. (1) is the higher-order energy contribution and is approximated as

$$\Delta E^r = - \sum_{i \in A} \sum_{j \in B} C_{ij}^6 R_{ij}^{-6} F_{ij}(R_{ij}), \qquad (3)$$

where

$$F_{ij}(R_{ij}) = \exp\left[-\left(1.28 R_{ij}^0 / R_{ij} - 1\right)^2 \right],$$

$$\text{if } R_{ij} \leqslant 1.28 R_{ij}^0,$$

$$= 1, \quad \text{elsewhere}, \qquad (4)$$

$F_{ij}(R_{ij})$ is a damping function introduced to correct the behavior of ΔE^r at short R_{ij} distance. R_{ij}^0 in Eq. (4) is the sum of van der Waals radii.
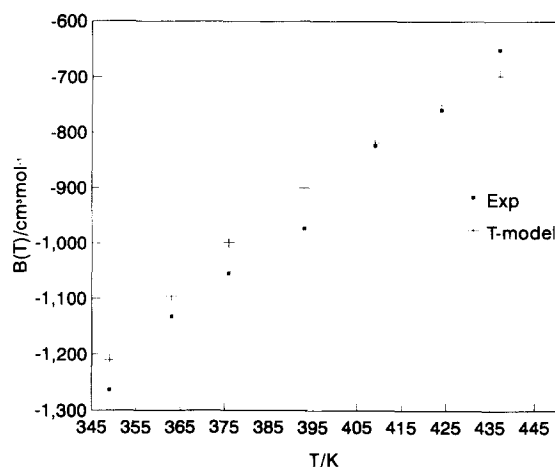

Fig. 1. Second virial coefficients of pyridine. Experimental $B(T)$ taken from Ref. [23].

The C_{ij}^6 parameters in Eq. (3) are computed from

$$C_{ij}^6 = C_6 \frac{3}{2} \frac{\alpha_i \alpha_j}{\left(\alpha_i / N_i\right)^{1/2} + \left(\alpha_j / N_j\right)^{1/2}}, \qquad (5)$$

where α and N are the atomic polarizabilities and number of valence electrons, respectively. Eq. (5) is the Slater–Kirkwood relation [22]. For ΔE^r, only C_6 is unknown. The value of C_6 can be determined using various experimental data. Since the experimental second-virial coefficients ($B(T)$) are available for pyridine [23], the C_6 parameter was determined in the present study by a fit of the incomplete potential (including Eqs. (2) and (3)) to the experimental $B(T)$. The quality of the fit is illustrated graphically in Fig. 1. The optimal C_6 parameter for the T-model is 1.622. In our experience, the calibration of the T-model potential by adjusting C_6 to reproduce the experimental $B(T)$ helps make the thermodynamic properties deduced from the T-model potential more realistic. This can be seen from the previous MD simulations, in which the computed potential energies of liquids always agree well with experiments [2,3,18].

The basis set used in the ab initio and first-order calculations are tabulated in Table 1 with the contraction schema. The T-model potential parameters for pyridine are summarized in Table 2.

Table 1
Basis set and contraction schema employed in the T-model calculations

Atom	Basis functions	Contraction schema
N and C	8s, 4p	[5111]/[31]
H	4s	[31]
N_T	11s, 7p	[5111111]/[31111]

N_T = nitrogen test-particle.

Table 2
Parameters for the T-model potential of pyridine

Atom	σ_i	ρ_i	q_i [a]
N	1.1189	0.3121	−0.676
C_1	0.8842	0.2681	0.467
C_2	1.0456	0.3749	−0.549
C_3	0.3497	0.3709	0.308
H_1	0.1356	0.2620	0.043
H_2	0.0388	0.2528	0.201
H_3	0.1937	0.2484	0.044

[a] Values taken from Ref. [21].

2.2. Monte Carlo and molecular dynamics simulations

The T-model potential computed in the previous section was used in the statistical mechanical simulations. Pyridine is considered to be a large molecule, in which reasonable equilibrium structures of liquid can be obtained only when a large number of configurations are accumulated and analyzed. Since the intermolecular forces are not computed explicitly in MC, it is more economical to use MC to bring an ensemble of pyridine molecules to equilibrium at a given temperature. The equilibrated configurations can then serve as starting configurations in MD.
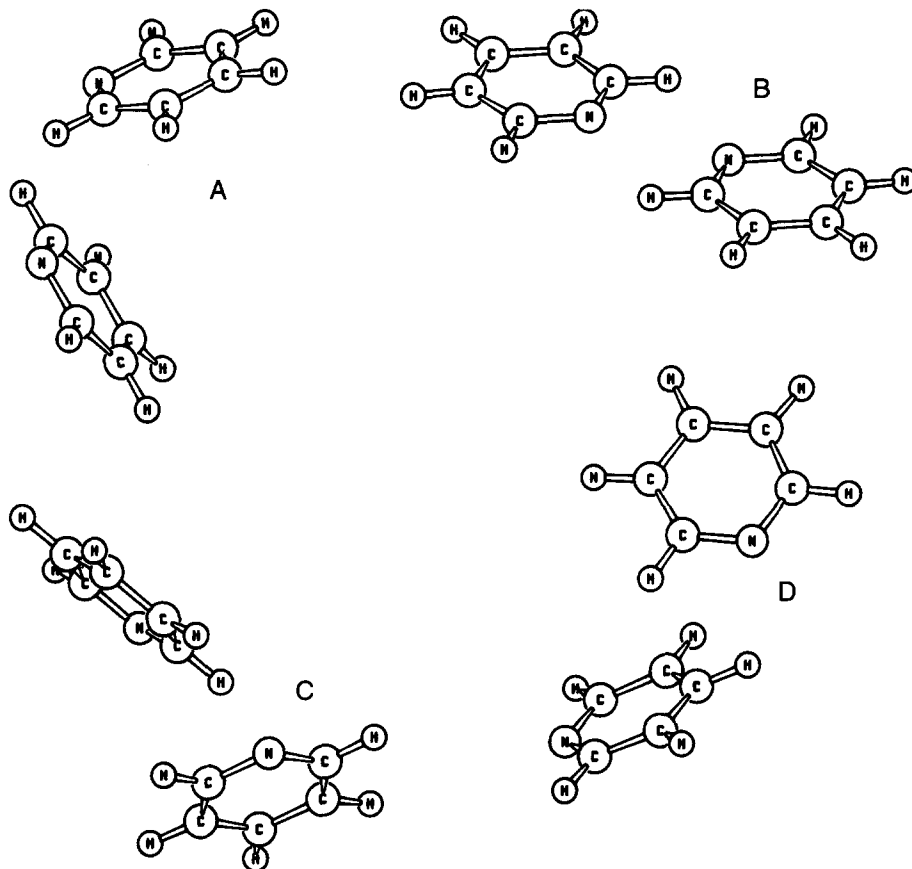

Fig. 2. Energy optimized pyridine dimer geometries obtained from the T-model potential. (a) $\Delta E = -13.416$ kJ/mol; (b) $\Delta E = -13.064$ kJ/mol; (c) $\Delta E = -12.252$ kJ/mol; (d) $\Delta E = -10.581$ kJ/mol.

Liquid pyridine was studied by considering 125 rigid pyridine molecules confined in a cubic box and subject to periodic boundary conditions. MC and MD simulations were performed in the temperature range of 230 to 360 K, with the liquid density fixed at 0.9819 g/cm³. The density employed is for liquid pyridine at 298.15 K [8]. The box length corresponds to the experimental density was 25.56 Å. About 500 000 MC steps were devoted to the equilibration, and another 500 000 steps for the static property calculations. For MD, the time step selected to solve the equations of motion was 0.005 ps. About 5000 time steps were devoted to ensure that the system was in equilibrium at each temperature. The dynamic properties were observed within 25 ps, starting from the equilibrated configurations. Dynamic properties of interest were the self-diffusion coefficients (D) and rotational diffusion constants (D_Ω). Self-diffusion constants were computed from the velocity autocorrelation functions, as well as from the mean square displacements. The structural properties computed from MC were the atom-atom pair correlation functions.

All calculations were made at DEC alpha 4710, computer at Suranaree University of Technology.

3. Results and discussion

In this section the equilibrium structures and energies of pyridine dimers, and the results of the statistical mechanical simulations are discussed.

3.1. Pyridine dimers

The T-model potential computed in the previous section was used in the geometry optimization of pyridine dimers. The computed equilibrium structures are shown in Fig. 2. Some characteristic atom–atom distances are listed in Table 3 and will be used in the discussion of the liquid structure. The absolute minimum of pyridine dimer is represented by a 'herringbone' like structure, with two symmetrical non-linear N · · · H–C hydrogen bonds (see Fig. 2a). Each pyridine molecule in this dimer seems to make efficient use of available chemical interactions within the molecule. The dipole moment of the C–N bond of each monomer is nearly antiparallel to each

Table 3
Characteristic interatomic distances for pyridine dimers

	Dimer configuration	Distance (Å)
N · · · N	A	4.197
	B	4.257
	C	4.946
	D	5.881
N · · · C	A	3.525
	B	3.562
	C	3.746
	D	3.586
N · · · H	A	2.895
	B	2.934
	C	3.076
	D	2.947
C · · · C	A	3.278
	B	3.291
	C	3.611
	D	3.457

other. The two N · · · H–C hydrogen bonds have the same N · · · C and N · · · H distances, 3.53 and 2.89 Å, respectively. The N · · · N distance for this herringbone structure is only 4.20 Å, shortest in comparison with the other pyridine dimers shown in Fig. 2. The dimerization energies computed by the T-model potential is −13.42 kJ/mol. A similar herringbone structure was previously found to dominate the solid pyridine [16].

Several local minimum energy geometries were predicted by the T-model potential namely, a parallel-displaced, a bent T-shaped, and an asymmetrical herringbone structure (see Figs. 2b, 2c and 2d, respectively). The interaction energies of these dimers are only slightly different from that of the herringbone structure. The energy differences seem not very significant, in comparison with the thermal energy fluctuation (RT) at room temperature. The parallel-displaced structure is stabilized by two non-linear N · · · C–H hydrogen bonds, with the C–N bond dipole moments antiparallel to each other. The bent T-shaped structure, in which two C–H groups of one monomer interact simultaneously at the N atom of the other, is only about 0.8 kJ/mol less stable than the parallel-displaced dimer. The asymmetrical herringbone structure is the least stable since it is stabilized by only one N · · · H–C bond.

Due to the size of aromatic moieties, the interactions between aromatic rings have not been studied extensively. It has been concluded that the dispersion interactions between aromatic rings could be the dominating factor in deciding the dimer structure [24], such as in benzene dimers. However, the situation is more complicated if two aromatic rings can form hydrogen bonds. The equilibrium geometry of benzene dimers was determined by computer modeling and discussed in comparison with the supersonic molecular jet laser optical spectroscopic results [7]. The computer modeling results were based on Lennard-Jones hydrogen bond (LJ-HB) potentials. The authors concluded that the parallel-displaced geometry with C_{2h} symmetry, slightly different from that shown in Fig. 2b, is the most stable form in the gas phase. The quadrupole–quadrupole interaction was reported to be responsible for the parallel-displaced geometry, with the energy of -10.82 kJ/mol. Based on the intermolecular potential deduced from MC simulations, Jorgensen and Severance [25] revealed that the T-shaped dimer is about 0.84 kJ/mol more stable than the paralled-displaced dimer. The most probable equilibrium geometry of phenol dimer was studied by analysis of rotational coherence spectra [24]. A dimer structure similar to the herringbone structure (Fig. 2a) was proposed to be the most stable dimer. It was pointed out that the electron density in the π-ring systems helps determine the structure of this complex. From the molecular structure and the value of the dipole moment of phenol, 1.22 D [8], one would expect similar equilibrium dimer structures for pyridine and phenol, in which the hydrogen bond and dispersion interactions favour the herringbone dimer geometry. Similar procedures were applied to determine the equilibrium geometry of pyrazine, pyrimidine and pyrazine–pyrimidine dimers [26–28]. It was found that the parallel-planar, parallel-stacked and T-shaped geometries are favored by these azabenzene dimers.

The above analysis confirms again that the dispersion interaction is, to some extent, responsible for the equilibrium dimer structures of benzene, phenol and azabenzene dimers. The hydrogen bond interaction will play a role for the molecules with non-zero dipole moment. The herringbone structure is just the result of the balance between the hydrogen bond and dispersion interactions.

3.2. Liquid pyridine

The computed potential energies of liquid pyridine at various temperatures are listed in Table 4. The atom–atom pair correlation functions derived from MC are shown in Fig. 3. The liquid potential energy at 312 K is predicted by MC to be -41.73 kJ/mol, in good agreement with that reported in Ref. [16] and the experimental heat of evaporation, 40.15 kJ/mol at 298 K [8].

Since the structures and peak locations of $g_{ij}(R_{ij})$ are quite similar for all temperatures, only the ones computed at 312 K are discussed in detail. $g_{NN}(R_{NN})$ and $g_{NH}(R_{NH})$ are the most structured. Therefore, they can be used to predict the average orientations of pyridine molecules in liquid. $g_{NN}(R_{NN})$ shows two well defined peaks at 4.79 and 6.00 Å. These peaks are close to the N $\cdots$ N distances found in the dimers C and D, respectively (see Fig. 2 and Table 3). A small shoulder is seen for $g_{NN}(R_{NN})$ at 4.15 Å. This short N $\cdots$ N distance is compatible with the N $\cdots$ N distance found in the herringbone dimer. $g_{NN}(R_{NN})$ suggests, therefore, that although the herringbone structure is predicted to be the most stable form in the gas phase, it is rarely found in the liquid. The types of the interactions similar to the dimers C and D seem to dominate in the liquid at 312 K. $g_{NH}(R_{NH})$ shows a well defined peak at 3.07 Å and a broad peak at 5.69 Å. The former is the N $\cdots$ H hydrogen-bonded distances. The latter is too long to be compared with the dimer configurations in Fig. 2. The number of pyridine molecules in the first and second solvation shells could not be determined easily from the running coordination numbers $(n_{ij}(R_{ij}))$. The integration of $g_{NN}(R_{NN})$ to the second minimum at 7 Å suggests about 11 pyridine molecules in the liquid. This is compatible with the MC results of liquid benzene, in which the coordination number of

Table 4
Potential energies of liquid pyridine derived from MC at various temperatures

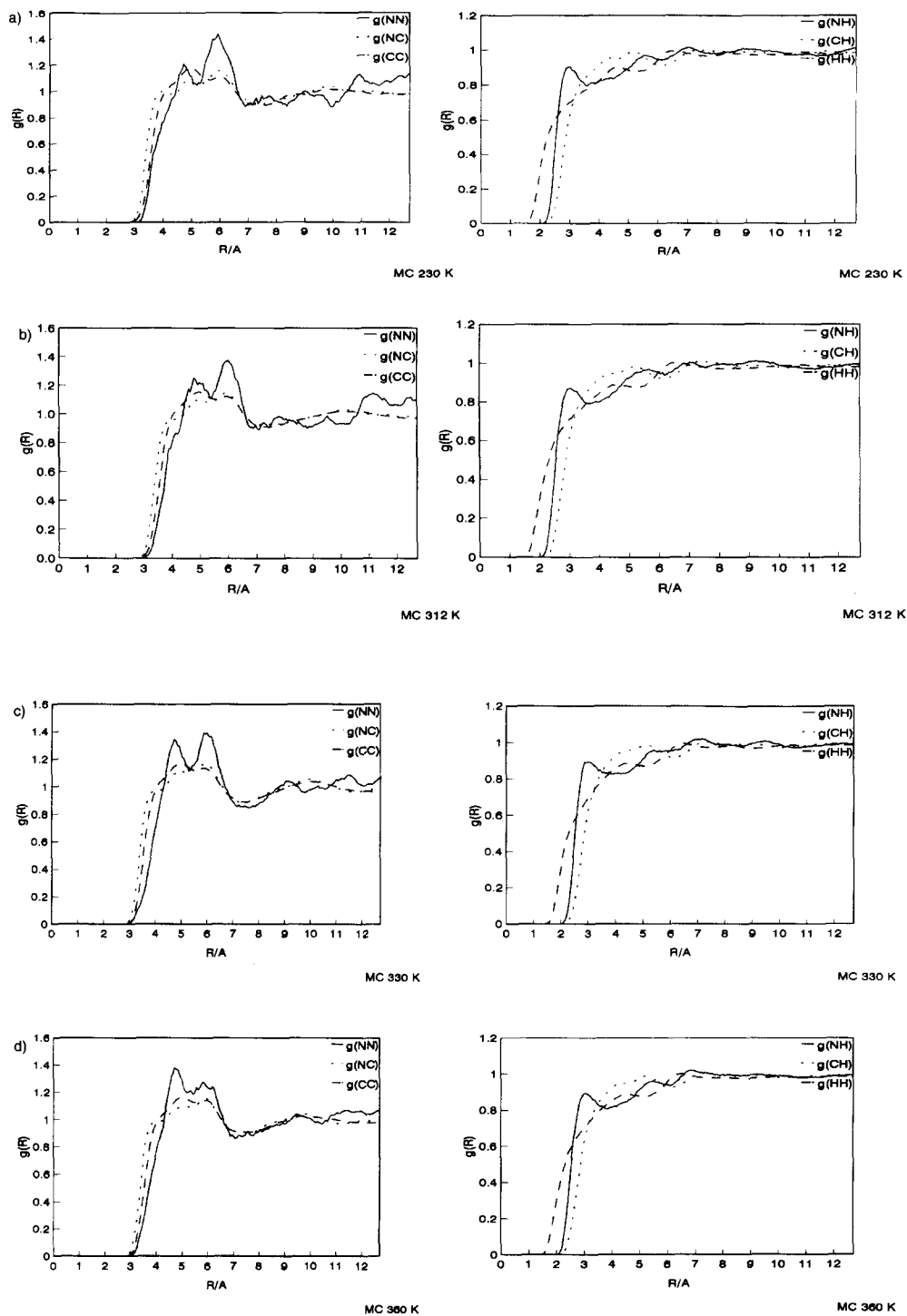| T (K)	E (kJ/mol)
230	-45.66
312	-41.73
360	-40.87

Fig. 3. Atom–atom pair correlation functions for liquid pyridine, (a) at 230 K; (b) at 312 K; (c) at 330 K; (d) at 360 K.

benzene was determined to be 12, by integration of the ring center–ring center pair correlation function to the minimum at 7.5 Å [25].

All peak locations and shapes of $g_{ij}(R_{ij})$ change only little when the temperature is varied from 230 to 360 K, except for the $g_{NN}(R_{NN})$. At 230 K, the first peak at 4.72 Å is smaller than the second at 5.94 Å. The integration of $g_{NN}(R_{NN})$ to the second minimum yields about 12 pyridine molecules in the liquid. The first peak becomes larger than the second peak at 360 K. Additional MC simulations were performed at 330 K to investigate the transition. At 330 K, the first and the second peaks have comparable size. This indicates that at low temperatures, there is a higher probability of finding geometries similar to the dimer C in comparison with D. The situation is reversed at temperatures higher than 330 K.

The atom–atom pair correlation functions reported by Gamba and Klein [16] show similar peak locations at 312 K. $g_{NN}(R_{NN})$ is slightly more structured than that computed in the present work. The first peak of $g_{NN}(R_{NN})$ is virtually smaller than the second for the liquid at 312 K, and the situation is reversed for solid pyridine at 159 K. The integration of $g_{NN}(R_{NN})$ to the second minimum yields 18 pyridine molecules in the liquid. The temperature dependence of $g_{NN}(R_{NN})$ cannot be discussed, since $g_{NN}(R_{NN})$ was shown at 312 K only.

The self-diffusion coefficients (D) derived from MD are listed in Table 5. The experimental self-diffusion coefficients for pyridine were reported based on nuclear relaxation measurements, in the temperature range from the freezing point to the normal

boiling points [15]. The values listed in Ref. [15] are represented by

$$D = (5.9 \pm 1.5)10^{-3}$$
$$\times \exp[-(3.45 \pm 0.15)/RT] \text{ cm}^2 \text{ s}^{-1}. \quad (6)$$

The energy term in Eq. (6) is in kcal/mol. The pre-exponential factor was theoretically estimated to be 2.5×10^{-3} cm^2 s^{-1} for pyridine. The self-diffusion coefficient for liquid pyridine was reported in Ref. [13] to be 1.88×10^{-5} cm^2 s^{-1} at 300 K. Comparison of the value with Table 5 reveals that our self-diffusion coefficient is smaller. It should be noted that the self-diffusion coefficients deduced from experiments were based on various approximations. Therefore, direct comparison with the present results seems not appropriate. Analysis of errors in Eq. (6), with the pre-exponential factors varying from 4.4×10^{-3} to 7.4×10^{-3} cm^2 s^{-1} and the exponents from $-3.3/RT$ to $-3.6/RT$, shows that, at 300 K, the values of D can vary from 1.05×10^{-5} cm^2 s^{-1} to 2.93×10^{-5} cm^2 s^{-1}. If the theoretical pre-exponential factor is used in Eq. (6), the self-diffusion coefficients will vary from 0.60×10^{-5} cm^2 s^{-1} to 0.99×10^{-5} cm^2 s^{-1}. It should be stressed that the self-diffusion coefficients computed from Eq. (6) are quite sensitive to the exponential term, which is related to the value of the activation energy. The error in the activation energy was estimated for the rotational correlation times (τ_2) to be ± 0.15 kcal/mol [15]. This is, in our opinion, rather small, compared with the thermal energy fluctuation (RT) at room temperature, 2.5 kJ/mol or 0.6 kcal/mol. The self-diffusion coefficients computed from Eq. (6), with the fluctuation in the activation energy of ± 0.6 kcal/mol, are in the range of 0.49×10^{-5} to 6.25×10^{-5} cm^2 s^{-1}. The values are closer to the results presented in Table 5.

The rotational diffusion coefficients (D_Ω) computed from MD are listed in Table 6, in comparison with the experimental values reported by Kintzinger and Lehn [9]. Our values at 300 K are in excellent agreement with the experiment [9]. The solid like region, in which the molecular rotations about the axis perpendicular to the molecular plane are faster than the motions about the in-plane axis, is predicted by MD to extend from 230 K to 360 K. The anisotropy of these motions increased slightly as the

Table 5
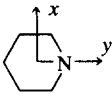The self-diffusion coefficients (D) for pyridine computed from MD

Temperature (K)	D^{msd} (10^{-5} cm^2 s^{-1})	D^{acf} (10^{-5} cm^2 s^{-1})
231	0.18	0.31
300	0.46	0.44
360	0.78	0.84

D^{msd}: self-diffusion coefficients computed from mean square displacements.
D^{acf}: self-diffusion coefficients computed from velocity autocorrelation functions.

Table 6
The rotational diffusion constants (D_Ω) for liquid pyridine derived from MD, compared with those reported in Ref. [9]

	Temperature		
	231 K	300 K	360 K
D_{Ω_x} $(\times 10^{10}$ s$^{-1})$	4.9	8.5 (8.5)	11.5
D_{Ω_y} $(\times 10^{10}$ s$^{-1})$	5.7	8.9 (8.5)	12.9
D_{Ω_z} $(\times 10^{10}$ s$^{-1})$	7.1	12.6 (13.0)	18.7
$D_{\Omega_x}/D_{\Omega_z}$	0.69	0.67	0.61
$D_{\Omega_y}/D_{\Omega_z}$	0.80	0.71	0.69

Values in parentheses were taken from Ref. [9].

temperature increased. This contradicts the results reported in Ref. [9], in which the anisotropy in the molecular rotations decreased at high temperatures. It should be noted that the analysis made in Ref. [9] depends largely on the experimental accuracies and the theoretical model employed. Kintzinger and Lehn [9] mentioned that the rotational diffusion model to describe the molecular motions of liquid pyridine is less valid at high temperature, especially for the rotations about the perpendicular axis. Further experimental results are therefore needed to clarify the temperature effects on the reorientational behavior of liquid pyridine.

4. Conclusion

In the present report, the T-model potentials were constructed for pyridine and used in the study of equilibrium dimer structures. Based on the dimerization energies, it was concluded that a herringbone structure is the most stable dimer in the gas phase. This, however, does not rule out the possibility of finding other local minimum energy geometries, since the energy differences are within the thermal energy fluctuation at room temperature. The conclusion is in reasonable agreement with all theoretical and experimental results on similar systems. There was no direct evidence from MC showing that the herringbone structure exists in an appreciable amount in the liquid phase. The self-diffusion coefficients computed from MD compared well with the experimental values, and are within reasonable experimental error for the activation energy. The MD results also showed that the molecular motions of liquid pyridine are rather anisotropic. This is in line with the experimental investigation on the reorientational motion reported by Kintzinger and Lehn. The computed dynamic properties could not be compared extensively since there is not enough reliable information on the experimental side. The authors believe, however, that the theoretical results reported here lead to reasonable pictures of molecular arrangements of pyridine in the gas and liquid phases which are difficult to obtain from experiment alone. These theoretical results should also lead to a better insight on the nature of the intermolecular interactions by which the behavior of molecules is dictated.

References

[1] H.J. Boehm and R. Ahlrichs, J. Chem. Phys. 77 (1982) 2028.
[2] K. Sagarik, R. Ahlrichs and S. Brode, Mol. Phys. 57 (1986) 1247.
[3] K. Sagarik and R. Ahlrichs, J. Chem. Phys. 86 (1987) 5117.
[4] K. Sagarik, V. Pongpituk, S. Chaiyapongs and S. Sisot, Chem. Phys. 156 (1991) 439.
[5] H.J. Boehm, C. Meissner and R. Ahlrichs, Mol. Phys. 53 (1984) 651.
[6] S. Warren, Workbook for organic synthesis (Wiley, New York, 1982).
[7] M. Schauer and E.R. Bernstein, J. Chem. Phys. 82 (1985) 3722.
[8] Handbook of chemistry and physics, 72th Ed. (CRC Press, Boca Raton, 1991).
[9] J.P. Kintzinger and J.M. Lehn, Mol. Phys. 22 (1971) 273.
[10] W.M. Litchman, J. Magn. Res. 14 (1974) 286.
[11] E.V. Goldammer and H.G. Hertz, J. Phys. Chem. 74 (1970) 3734.
[12] B. Parbhoo and O. Nagy, J. Mol. Struct. 177 (1988) 393.
[13] M. Fury, G. Munie and J. Jonas, J. Phys. Chem. 70 (1979) 1260.
[14] T. Ade, A. Hermann, V. Hoffmann and J. Weiss, J. Mol. Struct. 177 (1988) 367.
[15] D.E. O'Reilly, E.M. Peterson and E.L. Yasaitis, J. Chem. Phys. 57 (1972) 890.
[16] Z. Gamba and M.L. Klein, Chem. Phys. 130 (1989) 15.
[17] K. Sagarik, G. Corongiu and E. Clementi, J. Mol. Struct. THEOCHEM 235 (1991) 355.
[18] Y.P. Puhovski and B.M. Rode, J. Chem. Phys. 1994, in press.
[19] D.E. Williams, J. Comput. Chem. 9 (1988) 745.
[20] D.E. Williams and R.R. Weller, J. Am. Chem. Soc. 105 (1983) 4143.
[21] M. Orozco and F.J. Lugue, J. Comput. Chem. 11 (1990) 909.
[22] J.O. Hirschfelder, C.F. Curtis and R.B. Bird, Molecular theory of gases and liquids (Wiley, New York, 1954).

[23] J.H. Dymond and E.B. Smith, The virial coefficients of pure gases and mixtures (Clarendon Press, Oxford, 1980).

[24] L.L. Connell, S.M. Ohline, P.W. Joireman, T.C. Corcoran and P.M. Felker, J. Chem. Phys. 96 (1992) 2585.

[25] W.L. Jorgensen and D.L. Severance, J. Am. Chem. Soc. 112 (1990) 4768.

[26] J. Wanna, J.A. Menapace and E.R. Bernstein, J. Chem. Phys. 85 (1986) 777.

[27] J. Wanna and E.R. Bernstein, J. Chem. Phys. 85 (1986) 3243.

[28] J. Wanna and E.R. Bernstein, J. Chem. Phys. 84 (1986) 927.